Analysis of the effects of different machining processes on sealing using multiscale topography

Raphaël Deltombe, Maxence Bigerelle, Abdeljalil Jourani

Analysis of the effects of different machining processes on sealing using multiscale topography

Raphael Deltombe[1], **Maxence Bigerelle**[1,2] **and Abdeljalil Jourani**[3]

[1] Laboratoire d'Automatique, de Mécanique et d'Informatique Industrielle et Humaine LAMIH, UMR CNRS 8201, Valenciennes, France
[2] Laboratoire de Thermique, des Ecoulements, de Mécanique et Matériaux en Mise en Forme et Production, TEMPO, EA 4542, Valenciennes, France
[3] Université de Technologie de Compiègne, Laboratoire Roberval, UMR 7337, Compiègne, France

E-mail: rdeltomb@univ-valenciennes.fr

Keywords: roughness, finishing, sealing

Abstract

This study characterizes seal performance using a multiscale analysis of surface topography. The performance of two surface morphologies is compared: the first one is obtained with machining only and leads to leakage while the second one is obtained with machining and superfinishing and prevents leakage. It is shown that conventional roughness analysis does not enable to identify the differences between both surfaces. Only the use of a new parameter, the order parameter, and the use of a multiscale analysis of surfaces enable to distinguish the studied surfaces and to identify leakage causes. These causes are checked using a numerical contact simulation. It is shown that microroughness plays a major role in leakage.

1. Introduction

Seals are widely used as technical devices to isolate two chambers at different pressures and minimize the flow of a fluid (liquid or gas) between them. Numerous numerical studies, based on analytical formulae or finite element simulations, were conducted in order to understand sealing and more particularly leakage (e.g. [1–4]). Calculating leakage remains an issue as it depends on the seal design parameters as well as on the operating conditions. Another important parameter is roughness. However, determining its impact on leakage is not a simple matter [5, 6]. As an example, Haruyama *et al* [7] studied the influence of surface roughness on leakage of a new metal gasket. They used a finite element method to develop the simulation solution. Using different arithmetic mean values ($1.5\ \mu\text{m} < R_a < 3.5\ \mu\text{m}$), they observed that, for a low axial force, changes in surface roughness caused a significant change in the leakage whereas, for a high axial force, no changes were detected. Okada *et al* [8] investigated the influence of surface profiles on leakage in surface activated bonded, used in microelectromechanical systems devices. They chose to characterize the topography of the surfaces using the root-mean-square roughness (R_q). Robbe-Valloire and Prat [9] underlined the fact that sealing performance is not only due to the amplitude of roughness (i.e. R_a) but also depends on the distribution of valley and crest altitudes. In order to detect significant peaks, they used a 'motif' concept. It enables to obtain waviness motifs. All these studies emphasized the influence of surface topography on sealing performance. However, no analyses were conducted on the relevant scale of analysis for the understanding of leakage phenomenon. Indeed, roughness parameters have to be assessed with the appropriate filter and cut-off length in order to help the understanding of sealing performance.

This paper is dedicated to the characterization of sealing of a dual action pump composed of a stainless steel rod and a carbide seat, through a multiscale analysis of surface topography. Different final surface conditions are tested for the rods. For the first one, leading to leakage, the rod is only machined while for the second one, preventing leakage, the rod is machined and then superfinished. The first section of this paper presents the materials and methods. The second one is dedicated to the results and discussion and is composed of three main parts. First, conventional roughness analysis is conducted on the surfaces. Then, multiscale roughness analyses are performed. Finally,

a deterministic numerical contact model is presented in order to analyze sealing phenomenon. The conclusions summarize the main findings of this paper.

2. Materials and methods

2.1. Specimens

The studied device is a dual action pump. The latter is composed of a stainless steel rod and a carbide seat. Under standard conditions, the fluid pressure can reach 97.5 bars and a fluid volume of 25 cm^3 is expelled at a frequency equal to 40 cycles per minute. The sealing between the inlet and outlet chambers is provided by a polymeric material held by a metal spring. This study aims at comparing two kinds of surface finishing of the rods. The first studied rod (TM) is only machined while the second rod (TMA) is machined and then superfinished using an stone abrasive machine. Then, both rods are treated using physical vapor deposition in order to increase wear resistance with thickness of 2 μm. Indeed, the coating process applies a uniform thickness on the rod without modifying the whole roughness. After one hour of use, the TM/seat assembly leaks while the TMA/seat assembly remains sealed.

2.2. Topography measurements

Topography measurements were made using ZYGO NewViewTM 7300 3D optical surface profilometer, which is a metrology system based on white light interferometry. In order to get a large field of view, low optic magnification was used (x5 objective). Low optic magnification induces poor numerical aperture. Numerical aperture characterizes the range of angles over which the system can emit or receive light. It varies between 0.13 for a x5 objective and 0.8 for a x100 objective. The higher the numerical aperture, the larger the light-gathering ability. This is especially important for the rods because less light is received further away from the edge. Lateral resolution is also affected by the numerical aperture. Following Sparrow criterion [10], the lateral resolution varies between 2.58 μm and 0.34 μm for a x5 objective and a x100 objective, respectively. In order to further increase the dimensions of the measured areas, stitching [11] with an overlapping of 20% was used. Stitching enables to obtain large areas from the assembly of several small measurements, without decreasing the lateral resolution. The length and width of each measurement are equal to 20 mm and 1.09 mm, respectively.

The specimens were carefully placed under the white-light interferometer. The rod edge was aligned with the x-axis of the motorized microscope table. Furthermore, autofocus along the z-axis was used in order to compensate any rotation along the y-axis. Figure 1 shows the topographical maps of the machined rod (TM) and machined and superfinished rod (TMA) and the corresponding maps after form removal using a polynomial of degree 3. All the following calculations were made on the corrected maps.

3. Results and discussion

3.1. Conventional roughness analysis

Surface roughness parameters were calculated using the measurements shown in figure 1. Table 1 shows the calculation results. The surface roughness parameters calculated for TM and TMA show no significant differences. Functional volume parameters are particularly used in tribological studies. These parameters are calculated using the Abbot-Firestone curves or areal material ratio curve. Figure 2 illustrates the Abbot-Firestone curves obtained for the measurements shown in figure 1. The Abbot curves show similar trends: there are no obvious erosion peaks caused by superfinishing and no plateau morphology either. In order to investigate texture, angular power spectra were built. These are obtained by integrating the Fourier spectra in polar coordinates. The privileged direction corresponds to the angle showing the largest power spectrum. Figure 3 depicts the polar spectra obtained for TM and TMA. It can be seen that the studied surfaces show similar textures.

The comparisons of the surface roughness parameters, the Abbot curves and the polar spectra do not enable to understand the causes of leakage. Further analysis must be led. Figure 4 shows the autocorrelation function of TM and TMA and the corresponding two-dimensional autocorrelation functions computed in the y-direction i.e. in the leaking direction. The autocorrelation function of the superfinished surface has a periodic structure with peaks having small amplitudes. The periodic structure corresponds to the machining step (0.2 mm). This structure, embedded inside the macroscopic topography, was not revealed when using more conventional analysis means (roughness parameters, angular spectrum…). Figure 4 also shows that the rod called TMA has a larger periodic component than the rod referred to as TM, in the leaking direction. Thus, surface regularity plays an important role in preventing leaking and is perfectly revealed by ACF rather than by spectrum. However, The spectra method is precise in term of frequencies and less precise in term of distance (period). In the case of roughness, the distance is the unit of interest that's why autocorrelation find the period of the process when the spectrum fails.

Consequently, the parameter created by Bigerelle *et al* [12] was used. The last is scale-independent and thus enables to compare the order of surfaces at different scales of range and amplitude, in order to quantify the influence of different processes on the topography of the surface [13]. The main idea is to find a parameter without resorting to Fourier analysis because (i) spectrum parameters have little robustness and (ii) sine–cosine basis is not always appropriate for the

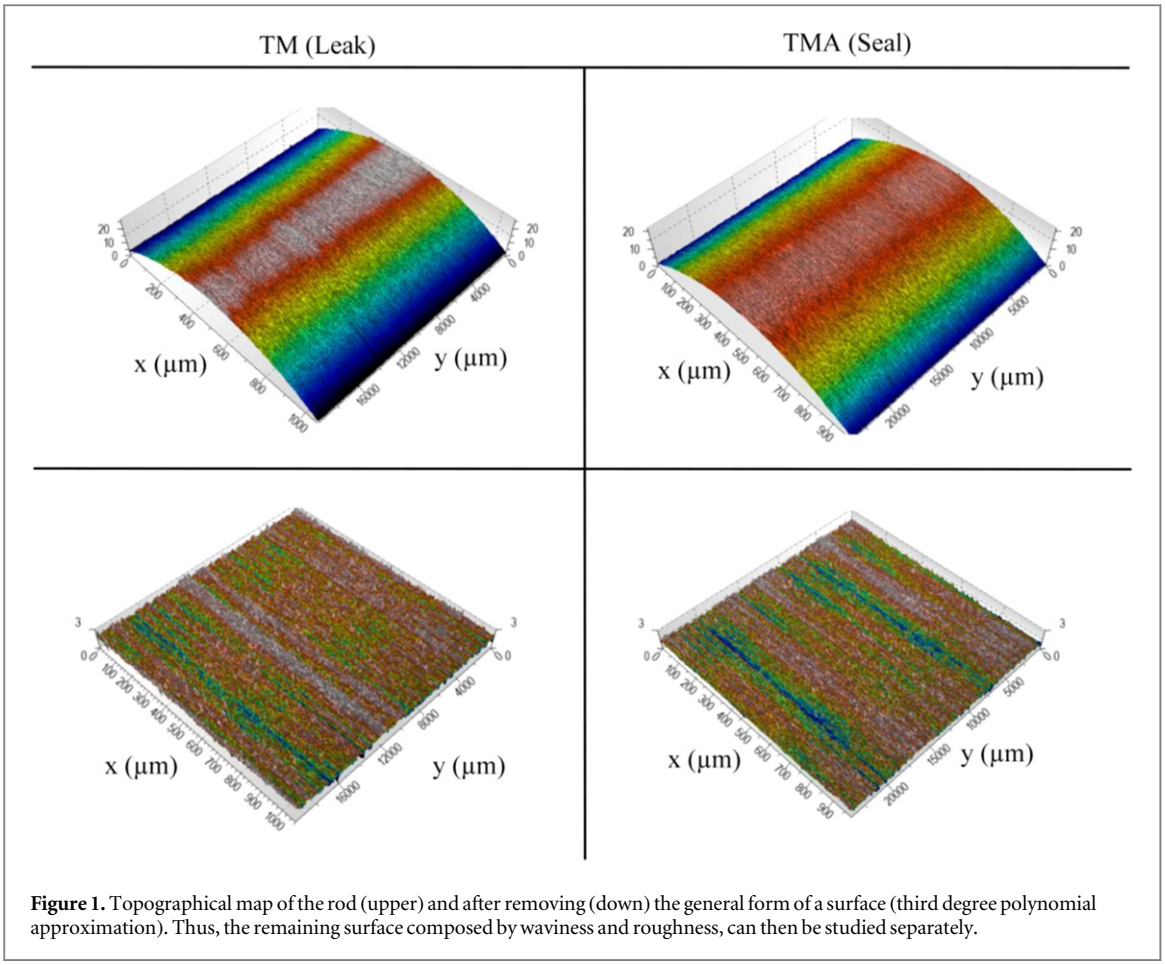

Figure 1. Topographical map of the rod (upper) and after removing (down) the general form of a surface (third degree polynomial approximation). Thus, the remaining surface composed by waviness and roughness, can then be studied separately.

Table 1. Main surface parameters for TM and TMA.

3D roughness parameters				
Symbol	Units	Name of parameter	TM	TMA
Amplitude parameters				
S_q	μm	Root mean square height	0.392	0.298
S_{sk}	—	Skewness	0.168	0.136
S_{ku}	—	Kurtosis	4.16	4.62
S_p	μm	Maximum peak height	2.09	1.74
S_v	μm	Maximum pit height	1.88	1.64
S_z	μm	Maximum height	3.98	3.38
S_a	μm	Arithmetic mean height	0.301	0.224

characterization of surface roughness. The scale-independent parameter must have:

(i) an upper limit value (100%) if surfaces are periodic,

(ii) a medium value for surfaces that have a non-negligible first-order autocorrelation,

(iii) a lower limit value equal to zero for uncorrelated random surfaces (white noise).

Firstly, a normalized autocorrelation function is defined by profiles extracted from three dimension surface in the leak direction. Then for each profile, the integer i is found using the following equation:

$$R(i) = \frac{1}{R_q^2(N-i)} \sum_{j=1}^{N-i} z_j z_{j+i} > 0.1, \tag{1}$$

where z_i are equidistant discretized amplitude points among N points and R_q is the standard deviation of the amplitude. Secondly, an autocorrelation length L and a correlation integral J are defined as follows

$$L = x_{i+1}, \tag{2}$$

$$J = \int_{x=0}^{x=L} R(x)\,\mathrm{d}x, \tag{3}$$

where the correlation integral J represents a sort of fundamental with regard to a function symbolizing a certain order power. Thirdly, the K series of I_k integrals is defined:

$$I_k = \int_{x=kL}^{x=(k+1)L} |R(x)|\,\mathrm{d}x. \tag{4}$$

It represents a kind of successive harmonics of the power order of profiles. Finally, the order parameter is defined as follows:

$$\text{order} = 100 \sum_{k=1}^{K} I_k/(K.\,J). \tag{5}$$

The order parameter lies between 0 (white noise profiles) and 100 (perfect periodic profiles without any noise). The most important quality of this parameter is to be mathematically independent of the amplitude

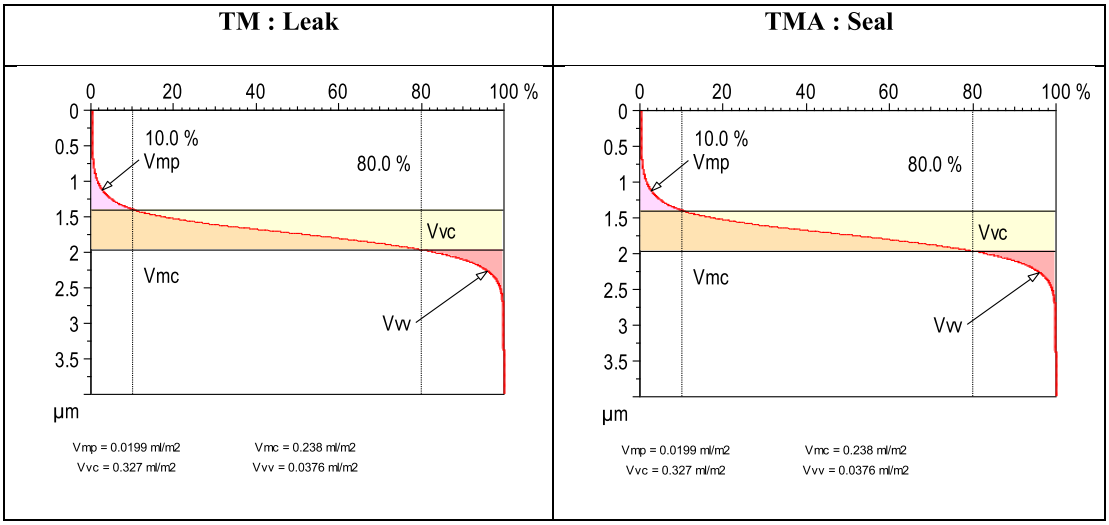

Figure 2. Abbott-Firestone curve (areal material ratio curve) calculated on the both surfaces shown on figure 1.

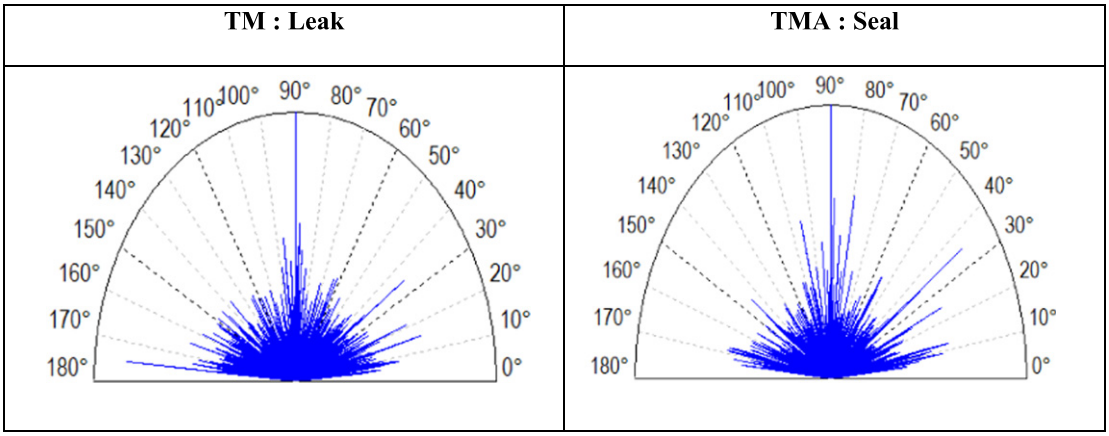

Figure 3. Anisotropy polar graphs calculated on the both surfaces shown on figure 1.

parameter and of the autocorrelation length of the surface. Therefore, the order of the surface and both the scaled parameter amplitude and autocorrelation can be analyzed to study scale effects without correlation bias. This parameter can also be extended from one-dimension to two-dimensions (x, y) for the measurement of the anisotropy of a surface [14].

Figure 5 shows the order function in the leaking direction for TM and TMA. The average value of the order parameter is equal to 5.5% for TM and 8.5% for TMA. Thus, the rod preventing leaking has a larger order parameter than the rod showing leaking. It seems that the repeated pattern perpendicular to the leaking enhances sealing. The non-superfinished surface also occasionally shows these barriers, as can be seen in figure 4. A possible explanation is that superfinishing does not affect roughness deeply. It enables to 'regulate' roughness by deeply enhancing periods induced by conventional machining.

The previously studied roughness parameters, as well as the Abbot-Firestone curve and the anisotropy polar graphs did not show any differences between the studied ropes. Only the order parameter enabled to identify the causes of leaking.

3.2. Multiscale roughness analyses

3.2.1. Basic aspects

The previous section showed that surface topography can caused leakage due to the loss of local barriers structures. However, all the tested roughness parameters failed to describe this structure when performing the analyses on the whole scale. This is why this section is dedicated to multiscale roughness analysis, using wavelet decomposition. A statistical method enabling to find the most relevant scale for the study of leaking is also presented. The multiscale analysis is made using two-dimensional data in the leaking direction because the measurements are larger (20 000 μm versus 1000 μm in the direction perpendicular to leaking). Indeed, the multiscale analysis requires sufficient length range.

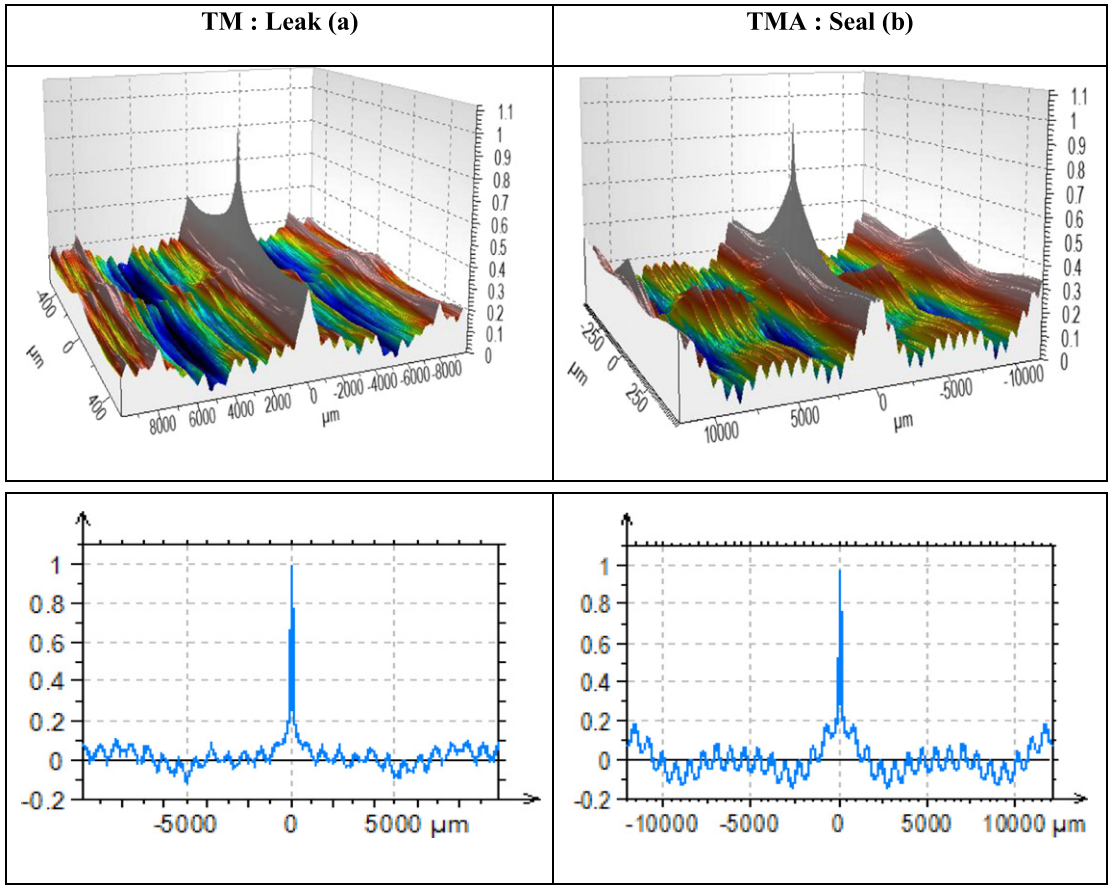

Figure 4. Autocorrelation function of surface TM (a) and TMA (b) rods. The 2D correlation functions computed in the *y*-direction (leak direction).

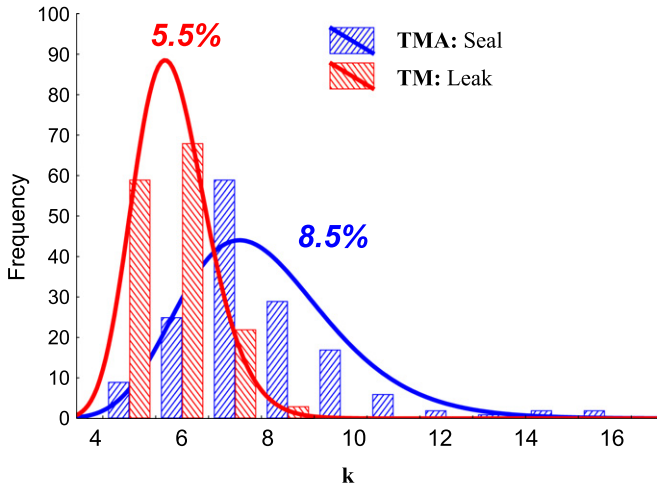

Figure 5. Order function (equation (5)) for TM and TMA surfaces in the leak direction (from figure 1).

3.2.2. The wavelet decomposition

Wavelets are often used to analyze multiscale aspects and more particularly the fractal aspects of abrasion [15–17]. The purpose is to find how the scales play an important role in leakage. First, the different shapes of the wavelets used to analyze the multiscale aspects of signals are presented. Different shapes of wavelets are retained in order to analyze their effects on signal characterization. Particularly, different Debauchies' wavelets are used with different orders (1, 2, 3, 4, 5, 7, 10, 15, 20, 25). It introduces various shapes due to an increase of wavelet oscillation with its order. Coiflets,

Symlets, Meyer and Bioorthogonal ones are also used. Three types of multiscale decomposition are proposed for the characterization of topography:

(i) roughness, which is defined by the lowest wavelet width summation as the B decomposition,

(ii) the waviness, which is defined by the highest wavelet width summation as the A decomposition,

(iii) the classical decomposition D (details), which corresponds to a given decomposition with a unique wavelet width.

Figure 6 displays the wavelet decomposition of the topography of the surface for TM and TMA. As it can be observed, multiscale spectra depend on the chosen wavelet. It is worth noting that the Meyer wavelet seems to well decompose the effect of the order described in the previous section. The changes seem to be localized by this wavelet over a bandwidth ranging from 500 μm to 2000 μm. For the topography showing no leaking, the spectrum is well described over this bandwidth and presents a period near to those met when using the macroscopic autocorrelation function. On the contrary, for the profile showing leaking, the periodicity is not well-defined. These spectra seem to confirm the previous macroscopic analyses. The next section is dedicated to the quantification of these observations.

3.2.3. The relevant wavelet and scale selection

Various authors reported that the choice of a wavelet shape is the most important step in wavelet analysis because it guarantees an accurate decomposition of the original signal into different frequency resolutions. The criterion for choosing the mother wavelet that best suits the signal depends strongly on the studied physical process. The most successful method consists in choosing the mother wavelet that best matches the shape of the analyzed signal [18–20]. As described in section 3.2.2, each profile is decomposed into a series of multiscale profiles (high frequency (B), low frequency (A) and details (D)) from which each roughness parameter can be computed. The following notations are used: the parameter $q_i(\varepsilon, w, d, k, n)$ represents the roughness parameter q_i computed from the nth profile taking into account K leaking conditions (leaking or no leaking), which is then transformed using a decomposition d with a wavelet shape w of width ε.

The main issue is to find the answers to the following questions:

(i) How to find the scale that gives the highest roughness differences between groups of specimens,

(ii) Which roughness parameter best quantifies this difference if one is significant,

(iii) Does this difference depends on the shape of the wavelet used to practice the decomposition,

(iv) What is the most relevant method of filtering (details, high, or low frequency signals)?

A statistical method is used to answer these questions. The most relevant scale is sought using an analysis of variance, which is an implementation of the generalized linear model. The following formalism is used:

$$q_i(\varepsilon, w, d, k, n) = \alpha_0(i, w, d, \varepsilon) + \alpha_k(i, w, d, \varepsilon) + \xi_{k,n}(i, w, d, \varepsilon), \tag{6}$$

where $q_i(\varepsilon, w, d, k, n)$ is the roughness parameter value of the nth profile when the p-leaking condition at level k ($k =$ leaking or no leaking) for a scale decomposition ε with a filtering d computed with a wavelet w. The parameter $\alpha_k(i, w, d, \varepsilon)$ is the influence of the leaking condition on the roughness parameter at k level, $\alpha_0(i, w, d, \varepsilon)$ is the mean level and $\zeta_{k,n}(i, w, d, \varepsilon)$ is a Gaussian noise with a null average value and a standard deviation of σ.

All the previous influences are calculated using an analysis of variance, for each wavelet w, each of the three types of filter d and each scale ε. Between-group variability and within-group variability (corresponding to errors of estimation of the roughness parameters into each group) are also calculated. The result noted $F(q_i, w, d, \varepsilon)$ is the ratio produced by dividing the between-group variability by the within-group variability. In other words, this result compares the effect of each process parameter on the roughness parameter value with its estimation error. As a consequence, a value of Fisher-criterion $F(q_i, w, d, \varepsilon)$ close to 1 for a given process parameter, means that the roughness parameter q_i computed for a given length ε is irrelevant for the description of the effects of leaking. The higher the $F(q_i, w, d, \varepsilon)$ value, the more relevant the parameter q_i computed at the scale ε [21].

The most relevant roughness parameter (computed at a given scale ε) for the description of leaking corresponds to the one having the largest $F(q_i, w, d, \varepsilon)$ value. Then, a bootstrap method [22] is applied to quantify the variability of the computed $F(q_i, w, d, \varepsilon)$ value. Figure 7 represents the analysis of the relevance function $F(q_i, w, d, \varepsilon)$, after classification of the values according to descending order. Thanks to the bootstrap (100 trials), a 90% confidence interval is plotted. The best result is found using the order parameter computed with Meyer wavelet using details decomposition at 625 μm. The second best result is found using the R_{pk} parameter with the same scale and wavelet but with a low-pass decomposition. Let's have a closer look at both parameters. Figure 8 depicts the order parameter as a function of the wavelet level for both surfaces (TM and TMA). The best relevance is found at 625 μm using a details decomposition. With

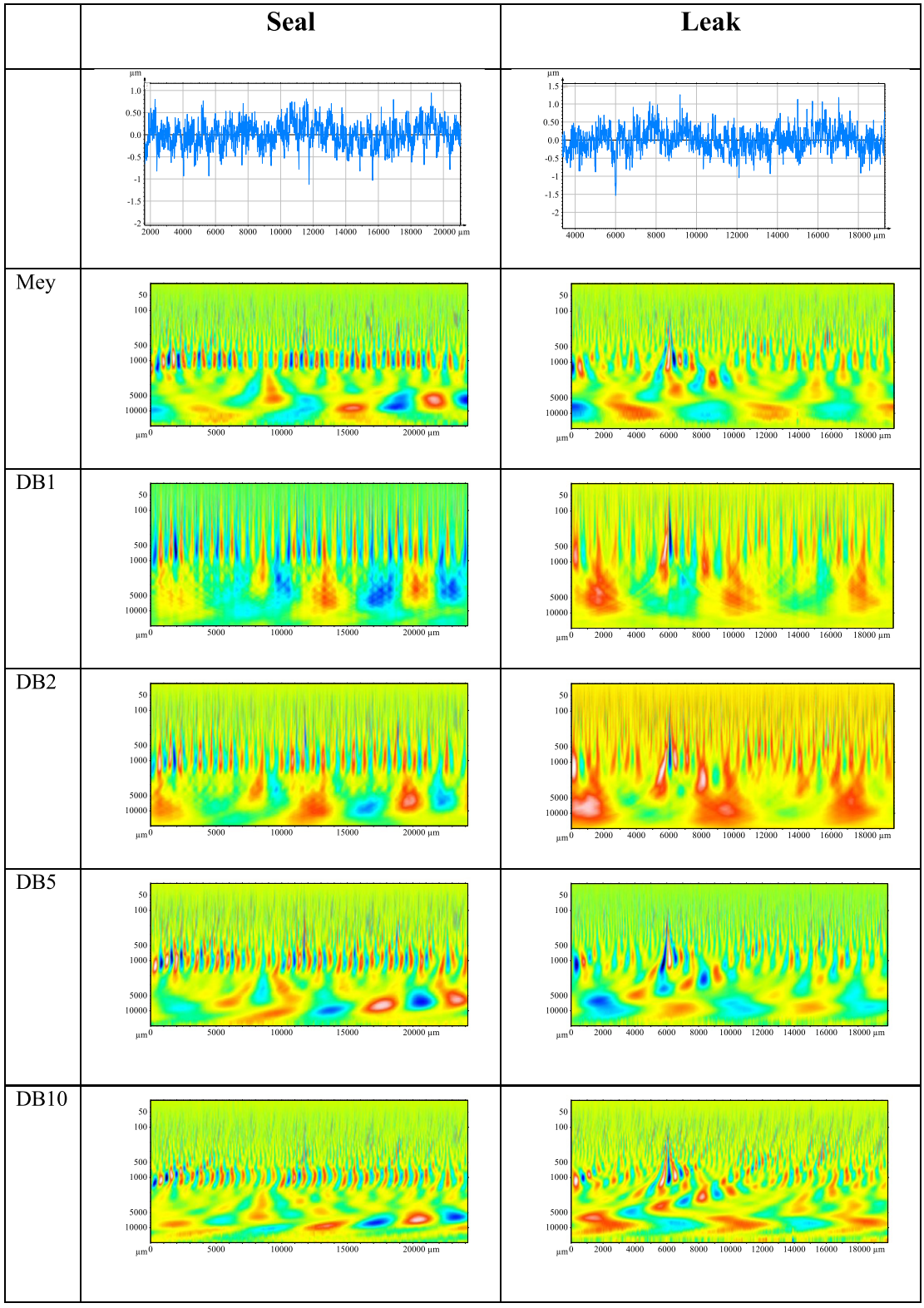

Figure 6. Multiscale decompositions of profile using Meyer wavelet, coiflet, symlet, Biorthogonal and Daubechies with different orders corresponding to the condition of fluid proof and leakage.

this configuration, the order parameter is approximately equal to 47% for the surface that shows no leaking while it is equal to 36% for the surface that shows leaking. These values confirm the previous results found with the macroscopic study. The values found with the multiscale study are higher than those obtained at the macroscopic level due to the fact that details decomposition deletes both high and low frequencies. This removal leads to a decrease of the quality of the autocorrelation function from which the order parameter is computed. This fact can be seen on figure 9, which illustrates the multiscale spectra

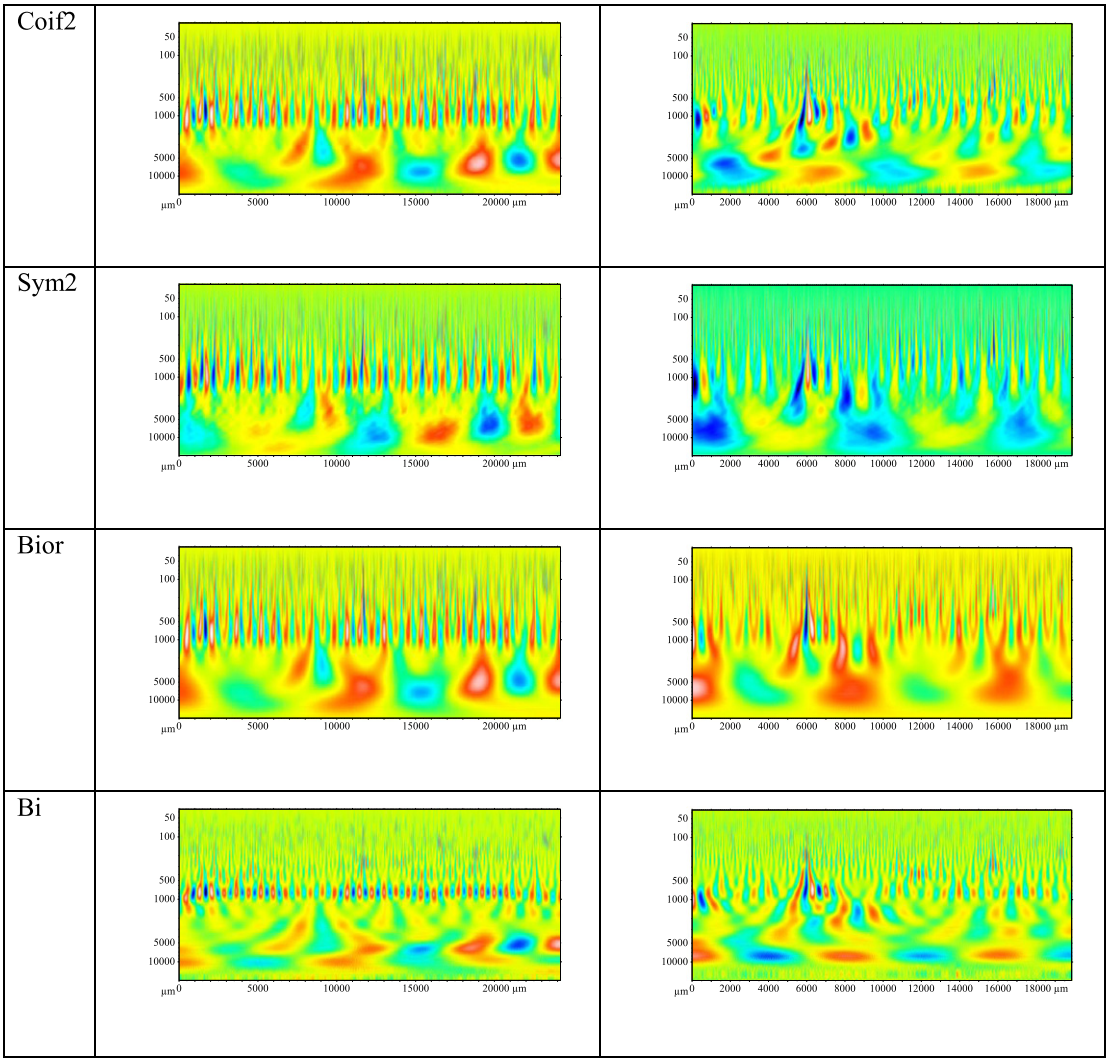

Figure 6. (Continued.)

obtained for the maximum level of relevance with Meyer wavelet. Figure 9 also shows the Abbot curves obtained for TM and TMA, computed using Meyer wavelet with details decomposition at 625 μm. Erosion peaks are observed for the polishing process. The corresponding R_{pk} values are equal to $0.08_{\pm 0.005}$ μm for the surface that shows no leaking and $0.23_{\pm 0.007}$ μm for the surface that shows leaking. On the contrary, the R_k and R_{vk} values are similar ($R_k \sim 0.30_{\pm 0.01}$ μm and $R_{vk} \sim 0.14_{\pm 0.007}$ μm). This clearly means that polishing erodes peaks without affecting the core and valley roughness. The multiscale analysis emphasizes the results obtained with the observation of the macroscopic roughness and allows a better investigation of the tribological mechanisms. The highest peaks are eroded by the abrasion process. This phenomenon gives a more periodical roughness that prevents leaking.

3.3. Contact/pressure model

The order parameter enables to quantify leaking. The previous analyses showed that leaking is closely related to surface anisotropy. In order to check this hypothesis, a three-dimensional contact model of asperities under loading is used [23]. The use of this model will help to determine the contact areas created when a macroscopic stress is applied.

3.3.1. Semi-analytical formulation

Roughness is modeled using a succession of asperities with a given distribution of attack angles. The definition of the average deformation is introduced by taking into account the average attack angle of the roughness $\bar{\beta}$.

The indentation by an axisymmetric indenter enables to estimate the stresses and strains undergoing in the indented material. For a given conical tip geometry, the mean pressure is linked to the attack angle β of the tip. Depending on the pressure supported by the summit, three regimes of deformation can be distinguished [24]. In the case of an elastic contact, the mean pressure supported by the asperity p^* can be written as follows:

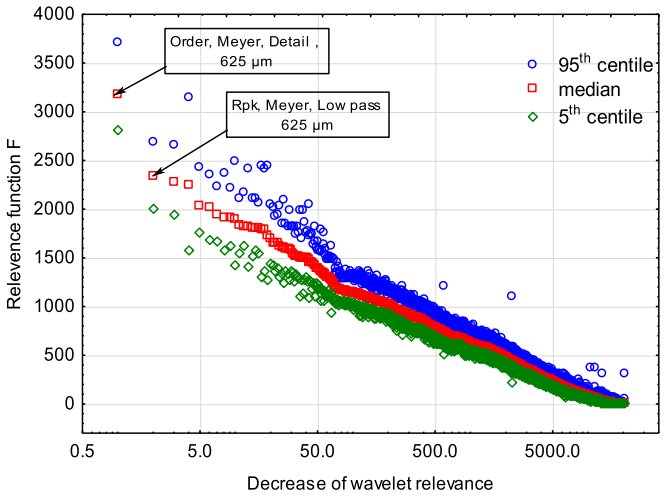

Figure 7. Analyses of the $F\left(q_i,\, w,\, d,\, \varepsilon\right)$ relevance function ordered by decreasing value. Thanks to the bootstrap (100 trials), 90% confidence interval is plotted. The order parameter is the best one (computed with Meyer wavelet in detail decomposition at 625 μm), and the second one is the R_{pk} one with the same scale and wavelet but in a low pass decomposition.

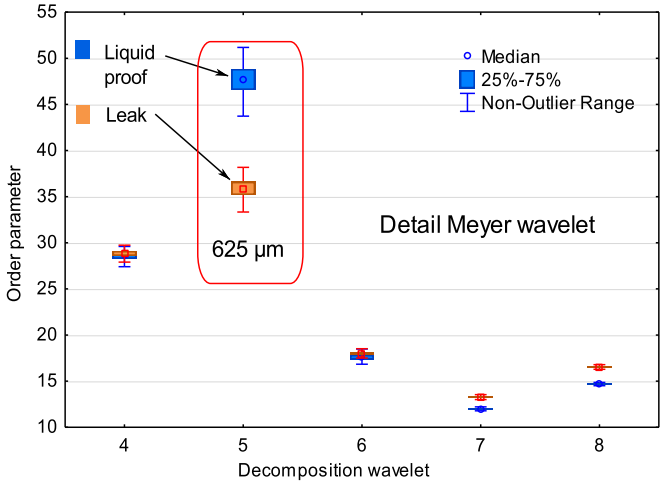

Figure 8. Multiscale graph plot of the order parameter obtained from a Meyer wavelet in details for the two surfaces with and without leaks.

$$p^* = 0.2E^* \tan \beta, \tag{7}$$

where E^* is the combined modulus of the two surfaces that are in contact.

If the contact is elasto-plastic, then the mean pressure p^* is given by:

$$p^* = \frac{2}{3}\left(1 + \ln \frac{E^* \tan \beta}{3\gamma}\right), \tag{8}$$

where γ is the yield limit.

When an asperity is plastically deformed, the mean pressure is given by the hardness H of the soft material [25]:

$$p^* \approx 3\gamma \approx H. \tag{9}$$

The local behavior of each asperity is numerically investigated using the local summits geometry analysis. In the latter, the contact between a perfectly smooth rigid plane and the local summits of the surface is considered and the elastic interactions between the asperities are neglected. The global contact area is decomposed into M local contact area. This local area A_j between an asperity j and the plane is assumed to be elliptic with semi-axes a_j and b_j and is given by [26]:

$$A_j = \pi a_j b_j. \tag{10}$$

In order to get numerical results, each local area in contact A_j is discretized into N c_{ji} elementary areas ($i = 1, 2, \ldots N$) in order to find that the sum of each c_{ji} is equal to A_j. With this discretization, the local pressure distribution on each local asperity j is given by the expression:

$$p_j\left(X_i,\, Y_i\right) = \frac{3}{2}p^*{}_j\left[1 - \left(\frac{X_i}{a_j}\right)^2 - \left(\frac{Yi}{b_j}\right)^2\right]^{1/2}, \tag{11}$$

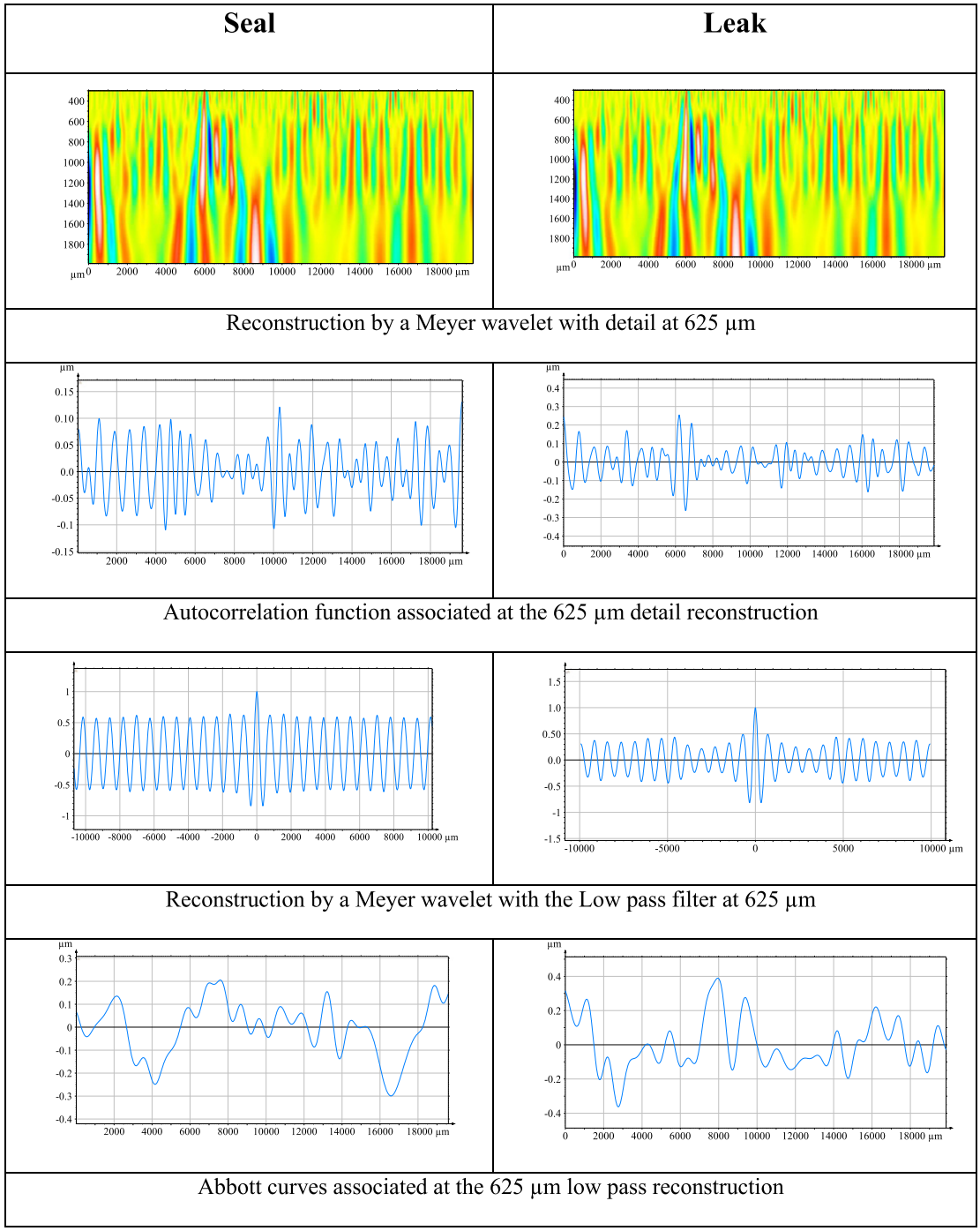

Figure 9. Zoom of multiscale spectra graphs at the maximal level of relevance for the Meyer wavelet. For the both surfaces (with or without leaks) , the autocorrelations functions (averaged on all profiles) and the Abbott curves averaged on all profiles) are plotted with a example of associated profile.

where p^*_j is the mean pressure undergone by the asperity j.

The normal force F_j acting on an asperity j is given by the following equation:

$$F_j = \sum_i^N c_{ji} p_i. \tag{12}$$

The total load supported by the summits is equal to:

$$F = \sum_{j=1}^{M} F_j, \tag{13}$$

where M is the number of asperities in contact.

The algorithm used for the contact calculation program is depicted in figure 10. The three-dimensional topography is directly sampled using the computed-generated surface topography [27]. For a given initial clearance δ, the local displacement δ_j, the local contact area A_j and the average attack angle β_i can be determined. These parameters enable to determine

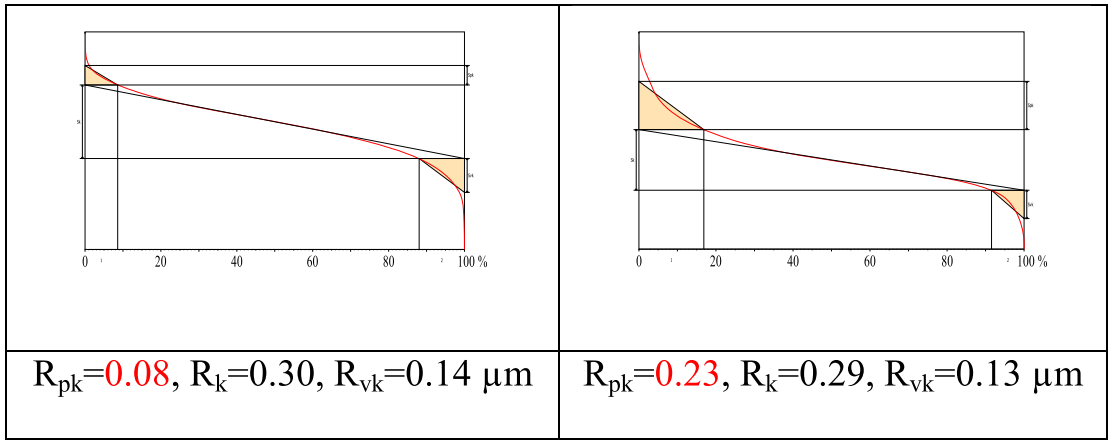

Figure 9. (Continued.)

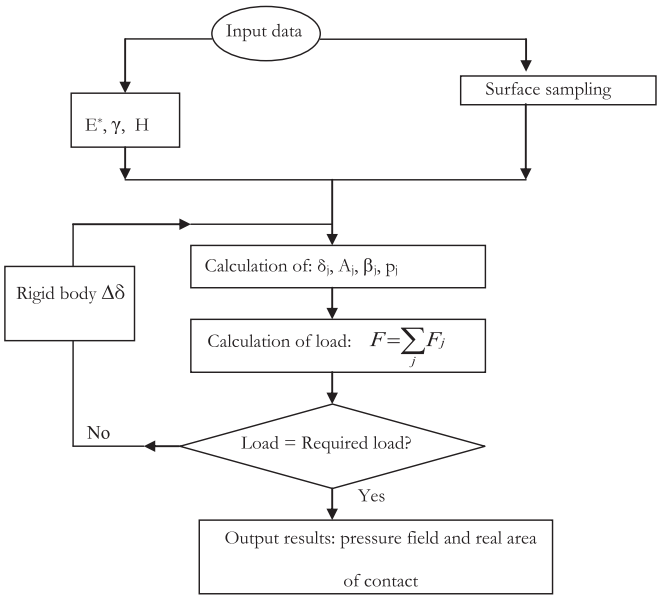

Figure 10. Flowchart for the numerical calculation of the pressure field and real area of contact.

the distribution of the pressure and also the real contact area of roughness. For a macroscopic displacement, the two surfaces are progressively brought into contact with several displacement increments $\Delta\delta$ of the smooth rigid plane. The displacement is interrupted when the resulting load F reaches the imposed normal force F_{max} (i.e. the convergence of the numerical software is reached).

3.3.2. Results of the model

A thorough examination of several pumps showed that using the pump does not induce any roughness change: no plastic deformations occur. Thus, it is not necessary to use an elastoplastic model for the simulation: the use of an elastic model is sufficient.

During operation, the superfinished surface (TMA) is perpendicular to the leaking barrier: sealing is ensured. At equal macroscopic pressure (20 MPa), the machined surface (TM) has perpendicular lines but they remain insufficient to prevent leaking (as shown in figure 11). Indeed, areas of fluid constriction are much scarcer on superfinished surfaces [28]. These results confirm the previous analyses.

Indeed, it was shown that leaking barriers are created by conventional machining. Then, these barriers are eroded by polishing thus generating infinite barriers preventing leaking. It is worth noting that the conducted investigations showed that ripples created by conventional machining also appear. This waviness is perpendicular to the flow. At the bottom of the waviness, microscopic roughness induced by the machining steps does not enable to prevent leaking. However, the microroughness located at the macroscopic height of the

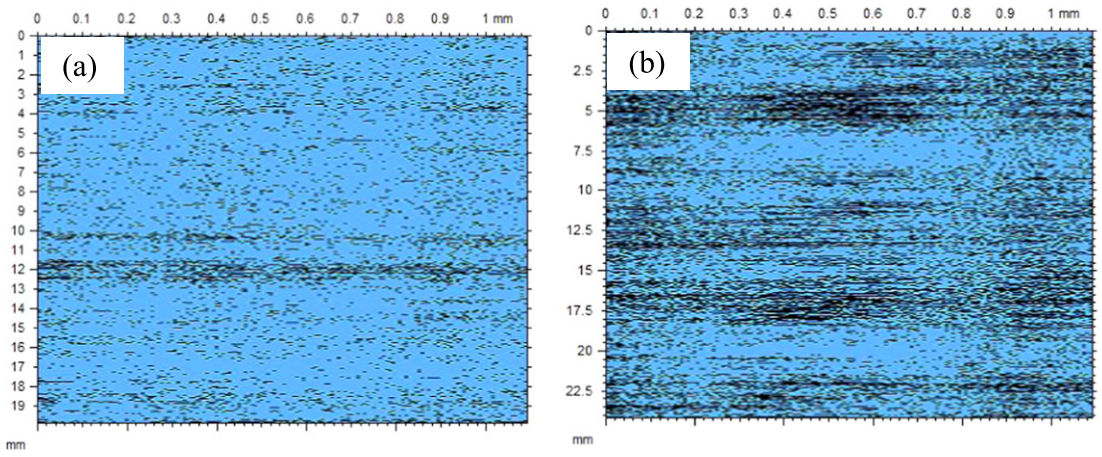

Figure 11. Fluid flow (blue) up and down through contact area (black) for TM (a) and for TMA (b).

waves crashes against the seal and form barriers that prevent leaking.

4. Conclusions

This study compared two kinds of surface finishing of rods used for sealing: the first studied rod (TM) was machined only and led to leaking, while the second rod (TMA) was machined and then superfinished and prevented leakage. Conventional roughness analysis did not enable to distinguish the studied surfaces. Similarly, the Abbot-Firestone curves and anisotropy polar graphs of TM and TMA showed no significant differences. The use of a new roughness parameter, the order parameter, enabled to distinguish the examined surfaces. It was shown that the rod preventing leakage had a larger order parameter than the one leading to leakage. It was found that a repeated pattern perpendicular to the leaking direction enhanced sealing. The superfinishing step enables to erode the peaks without affecting the core and valley roughness. It gives a more periodical roughness that prevents leaking. These observations were confirmed using a semi-analytic contact analysis.

Therefore, while contact pressure is linked to waviness, the microroughness structure should be carefully monitored in order to ensure perfect sealing. The structure should be mastered in order to create infinitely long barriers that enable to prevent leakage. Conventional machining creates these barriers and superfinishing ensures their consistency.

References

[1] Murali Krishna M, Shunmugam M S and Siva Prasad N 2007 A study on the sealing performance of bolted flange joints with gaskets using finite element analysis *Int. J. Press. Vessels Pip.* **84** 349–57

[2] Bottiglione F, Carbone G and Mantriota G 2009 Fluid leakage in seals: an approach based on percolation theory *Tribol. Int.* **42** 731–7

[3] Persson B N J, Albohr O, Tartaglino U, Volokitin A I and Tosatti E 2005 On the nature of surface roughness with application to contact mechanics, sealing, rubber friction and adhesion *J. Phys.: Condens. Matter.* **17** R1

[4] Minet C, Brunetiere N, Tournerie B and Fribourg D 2010 Analysis and modeling of the topography of mechanical seal faces *Tribol. Trans.* **53** 799–815

[5] Putignano C, Afferrante L, Carbone G and Demelio G P 2013 A multiscale analysis of elastic contacts and percolation threshold for numerically generated and real rough surfaces *Tribol. Int.* **64** 148–54

[6] Roth A 1970 The influence of the surface roughness on the specific leak rate of gasket seals *Vacuum* **20** 431–5

[7] Haruyama S, Nurhadiyanto D, Choiron M A and Kaminishi K 2013 Influence of surface roughness on leakage of new metal gasket *Int. J. Press. Vessels Pip.* **111–112** 146–54

[8] Okada H, Itoh T and Suga T 2008 The influence of surface profiles on leakage in room temperature seal-bonding *Sensors Actuators* A **144** 124–9

[9] Robbe-Valloire F and Prat M 2008 A model for face-turned surface microgeometry: application to the analysis of metallic static seals *Wear* **264** 980–9

[10] Leach R 2011 *Optical Measurement of Surface Topography* (Berlin: Springer)

[11] Murphy P, Forbes G, Fleig J, Dumas P and Tricard M 2003 Stitching interferometry: a flexible solution for surface metrology *Opt. Photonics News* **14** 38–43

[12] Bigerelle M, Anselme K, Dufresne E, Hardouin P and Iost A 2002 An unscaled parameter to measure the order of surfaces: a new surface elaboration to increase cells adhesion *Biomol. Eng.* **19** 79–83

[13] Bigerelle M, Anselme K, Noël B, Ruderman I, Hardouin P and Iost A 2002 Improvement in the morphology of Ti-based surfaces: a new process to increase in vitro human osteoblast response *Biomaterials* **23** 1563–77

[14] Guillemot G, Bigerelle M and Khawaja Z 2014 3D parameter to quantify the anisotropy measurement of periodic structures on rough surfaces *Scanning* **36** 127–33

[15] Mezghani S, Zahouani H and Piezanowski J J 2011 Multiscale characterizations of painted surface appearance by continuous wavelet transform *J. Mater. Process. Technol.* **211** 205–11

[16] Zahouani H, Mezghani S, Vargiolu R and Dursapt M 2008 Identification of manufacturing signature by 2D wavelet decomposition *Wear* **264** 480–5

[17] Bigerelle M, Guillemot G, Khawaja Z, El Mansori M and Antoni J 2013 Relevance of Wavelet Shape Selection in a complex signal *Mech. Syst. Signal Process.* **41** 14–33

[18] Petropulu A P 1992 Detection of transients using discrete wavelet transform *ICASSP-92, 1992 IEEE Int. Conf. on Acoustics, Speech, and Signal Processing* vol 2 pp 477–80

[19] Abbate A, Koay J, Frankel J, Schroeder S C and Das P 1994 Application of wavelet transform signal processor to ultrasound *1994 IEEE Ultrasonics Symp., Proc.* vol 2 pp 1147–52
[20] Rizzo P and Lanza di Scalea F 2004 Discrete wavelet transform to improve guided-wave-based health monitoring of tendons and cables *Smart Structures and Materials* (*San Diego*) vol 5391 pp 523–33
[21] Najjar D, Bigerelle M, Migaud H and Iost A 2006 About the relevance of roughness parameters used for characterizing worn femoral heads *Tribol. Int.* **39** 1527–37
[22] Najjar D, Bigerelle M and Iost A 2003 The computer-based bootstrap method as a tool to select a relevant surface roughness parameter *Wear* **254** 450–60
[23] Hagege B, Bouvier S, Mazeran P E and Bigerelle M 2011 3D finite element model of elastoplastic contact on the double sinus rough surface *J. Phys.: Conf. Ser.* **311** 1–5
[24] Johnson K L 1985 *Contact Mechanics* (Cambridge: Cambridge University Press)
[25] Tabor D 1951 *The Hardness of Metals* (Oxford: Oxford University Press)
[26] Ogilvy J A 1991 Numerical simulation of friction between contacting rough surfaces *J. Phys. D: Appl. Phys.* **24** 2098–109
[27] Jourani A, Dursapt M, Hamdi H, Rech J and Zahouani H 2005 Effect of the belt grinding on the surface texture: modeling of the contact and abrasive wear *Wear* **259** 1137–43
[28] Persson B N J and Yang C 2008 Theory of the leak-rate of seals *J. Phys.: Condens. Matter.* **20** 1–12